arXiv:astro-ph/9811014v1 2 Nov 1998

A Study of High Energy Emission from the TeV blazar Mrk 501 during Multiwavelength Observations in 1996

J. Kataoka[1,2], J. R. Mattox[3], J. Quinn[4], H. Kubo[5], F. Makino[1], T. Takahashi[1], S. Inoue[6], R. C. Hartman[7], G. M. Madejski[7,8], P. Sreekumar[7,9], and S. J. Wagner[10]

ABSTRACT

We present the results of a multiwavelength campaign for Mrk 501 performed in March 1996 with *ASCA*, *EGRET* , *Whipple*, and optical telescopes. The X–ray flux observed with *ASCA* was 5 times higher than the quiescent level and gradually decreased by a factor of 2 during the observation in March 1996. In the X–ray band, a spectral break was observed around 2 keV. We report here for the first time the detection of high-energy γ–ray flux from Mrk 501 with *EGRET* with 3.5 σ significance (E $>$ 100 MeV). Higher flux was also observed in April/May 1996, with 4.0 σ significance for E $>$ 100 MeV, and 5.2 σ significance for E $>$ 500 MeV. The γ–ray spectrum was measured to be flatter than most of the γ–ray blazars. We find that the multiband spectrum in 1996 is consistent with that calculated from a one-zone SSC model where X–rays are produced via synchrotron emission, and γ-rays via inverse Compton scattering of synchrotron photons in a homogeneous region. The flux of TeV γ–rays is consistent with the predictions of the model if the decrease of the

[1]Institute of Space and Astronautical Science, 3-1-1 Yoshinodai, Sagamihara, Kanagawa 229-8510, Japan

[2]Department of Physics, University of Tokyo, 7-3-1 Hongo, Bunkyo-ku, Tokyo 113-0033, Japan

[3]Astronomy Department, Boston University, 725 Commonwealth Avenue, Boston, MA 02215

[4]Fred Lawrence Whipple Observatory, Harvard-Smithsonian Center for Astrophysics, P. O. Box 97, Amado, AZ 85645-0097

[5]The Institute of Physical and Chemical Research, 2-1 Hirosawa, Wako, Saitama 351-0198, Japan

[6]Department of Physics, Tokyo Metropolitan University, 1-1 Minami-Osawa, Hachioji, Tokyo, Japan 192-0397

[7]Laboratory for High Energy Astrophysics, NASA/GSFC, Greenbelt, MD 20771

[8]Dept. of Astronomy, Univ. of Maryland, College Park, MD 20742

[9]Universities Space Research Association

[10]Landessternwarte Heidelberg, Kőnigstuhl, D-69117 Heidelberg, Germany

Compton-scattering cross section in the Klein-Nishina regime is considered. In the context of this model, we investigate the values of the magnetic field strength and the beaming factor allowed by the observational results. We compare the March 1996 multiwavelength spectrum with that in the flare state in April 1997. Between these two epochs, the TeV flux increase is well correlated with that observed in keV range. The keV and TeV amplitudes during the April 1997 flare are accurately reproduced by a one-zone SSC model, assuming that the population of synchrotron photons in 1996 are scattered by the newly injected relativistic electrons, having maximum energies of $\gamma_{max} \sim 6 \times 10^6$. However, the TeV spectrum observed during March 1996 campaign is flatter than predicted by our models. We find that this cannot be explained by either higher order Comptonization or the contribution of the 'seed' IR photons from the host galaxy for the first-order external radiation Comptonization, but we cannot exclude possible effects of the IR photons that may arise in the parsec-size torus postulated to exist in AGN.

Subject headings: keyword: BL Lacertae objects: individual (Markarian 501)−X–rays, γ–rays: observations

1. Introduction

Observations by the *EGRET* instrument (30 MeV – 30 GeV; Thompson et al. 1993) onboard the *Compton Gamma-Ray Observatory* (*CGRO*) reveal that γ–ray emission dominates the apparent power output for many blazar type Active Galactic Nuclei (AGN). About 50 sources detected with *EGRET* in the high-energy γ–ray band are identified with blazars (see, e.g., Mattox et al. 1997b; Mukherjee et al. 1997). The γ–ray emission extends up to TeV energies for three nearby blazars: Mrk 421 ($z = 0.031$; Punch et al. 1992; Petry et al. 1996), Mrk 501 ($z = 0.034$; Quinn et al. 1996; Bradbury et al. 1997; Aharonian et al. 1997) and 1ES 2344+514 ($z = 0.044$; Weekes et al. 1996; Catanese et al. 1998).

The overall electromagnetic spectra of blazars, when plotted in the νF_ν space, generally reveal two broad peaks; one located between IR and X–rays, and another in the γ–ray regime (e.g., von Montigny et al. 1995); in a few objects, additional components are observed in the IR/optical band, but those are probably not directly associated with the blazar phenomenon, but instead they are likely to be due to the isotropic emission of the associated AGN (e.g., Falomo et al. 1993). The models invoked to explain the radiative processes in blazars have these two components correspond to two different emission

processes from the same population of relativistic particles. The polarization observed in the radio and optical bands indicates that the lower energy emission is most likely due to the synchrotron process, while the inverse-Compton mechanism is thought to be dominant for the high energy γ–ray emission (see, e.g., Ulrich, Maraschi & Urry 1997). However, the source of the 'seed' photons for the Compton process is a matter of debate. In some models, it is synchrotron radiation internal to the jet — the Synchrotron-Self-Compton (SSC) model (Jones et al. 1974; Marscher 1980; Kőnigl 1981; Marscher & Gear 1985; Ghisellini & Maraschi 1989; Maraschi et al. 1992; Marscher & Travis 1996), while in others, it is radiation external to the jet — the External Radiation Compton (ERC) model (Dermer & Schlickeiser 1993; Sikora, Begelman, & Rees 1994).

Blazars are highly variable from radio to γ–ray bands: flares with time scales as short as 15 minutes have been observed in the TeV range (Gaidos et al. 1996). The correlation of variability between different bands can potentially discriminate between various models. The first TeV blazar that was observed simultaneously in multiple bands from radio to TeV γ–rays is Mrk 421. The first campaign, conducted in 1994 (Macomb et al. 1995), revealed correlated variability between the keV X–ray and TeV γ–ray emission, where the γ–ray flux varied by an order of magnitude on a time scale of 2 days and the X–ray flux was observed to double in 12 hours. On the other hand, the high-energy γ–ray flux observed by *EGRET* , as well as the radio and UV fluxes showed less variability than the keV or TeV bands. Another Mrk 421 multiwavelength campaign performed in 1995 revealed another coincident keV/TeV flare (Buckley et al. 1996; Takahashi et al. 1996b). Although the relative amplitudes of variability are different, the UV and optical bands also showed correlation during the flares. These results indicate that the high energy tail of the energy distribution of a single electron population is responsible for both the X–rays and TeV γ–rays (Takahashi et al. 1996a). With the detection of TeV emission from Mrk 501 (Quinn et al. 1996), several multi-band campaigns were organized to observe this object to verify if such a behavior is a general property of TeV-emitting blazars, or if it is unique to Mrk 421.

During the April 1997 multiwavelength campaign for Mrk 501, both X–rays and TeV γ–rays increased by more than one order of magnitude from quiescent level (Catanese et al. 1997; Pian et al. 1998). While the synchrotron emission peaked below 0.1 keV in the quiescent state, in 1997 it peaked at ~ 100 keV — the largest shift ever observed for a blazar (Pian et al. 1998); this is in contrast to Mrk 421, which shows relatively little variability of the position of the synchrotron peak (e.g., Macomb et al. 1995). Mastichiadis & Kirk (1997) suggest that the SSC scheme in a homogeneous region is sufficient to interpret the multiband spectrum of Mrk 421. They also suggest that the flare in 1994 is probably caused by a change in the maximum energy of electrons (γ_{max}). The origin of the April 1997 flare of Mrk 501 was also investigated by Pian et al (1998). They calculated that the variation

of the γ_{max} together with an increased luminosity and a flattening of the injected electron distribution can describe observed spectra well. Their model shows good agreement with the data, but does not reproduce the TeV γ-ray flux during the high state in April 1997.

The correlation between the high-energy γ–ray and other bands is important to study the radiation mechanisms of blazars. A combined GeV and TeV spectrum can place a strong limit on the high energy emission and its relation with the low energy emission. However, observations of HBLs (High-frequency-peaked BL Lac objects) in the high-energy γ-ray band from 30 MeV to several GeV are difficult because HBLs are faint in this energy band (e.g., Mukherjee et al. 1997). For instance, Mrk 421 is detected at a level comparable to the *EGRET* sensitivity (Fichtel et al. 1994; Thompson et al. 1995). Catanese et al. (1997) present an *EGRET* observation of Mrk 501 during the 1997 X-ray/TeV flare (Apr. 9 – 15), and report a 1.5 σ excess at the position of the source and furnish an upper limit.

In this paper we present Mrk 501 data from simultaneous March 1996 observations by *ASCA* (keV), *EGRET* (GeV) and *Whipple* (TeV), together with the optical observations. The *EGRET* observation during this campaign indicates a detection with 3.5 σ significance (E $>$ 100 MeV) during a 3.2 day interval of peak flux. Also, a month later, *EGRET* detected Mrk 501 with 4.0 σ significance (E $>$ 100 MeV; 5.2 σ for E $>$ 500 MeV). This is the first report of the detection of Mrk 501 by *EGRET* . The observations and analysis are presented in §2. The multifrequency spectra during the campaign are described and compared with the April 1997 flare state and a quiescent state in §3. We discuss the radiation mechanism of TeV blazar Mrk 501 in §4, and present our conclusions in §5.

2. Observations and Results

2.1. *ASCA*

We observed Mrk 501 four times with *ASCA* during 1996 March 21.3 − April 2.9 UT. Each pointing was about 10 ksec in duration. The observations were performed in a nominal, 1CCD mode for the Solid-state Imaging Spectrometer (SIS: Burke et al. 1991), and a nominal PH mode for the Gas Imaging Spectrometer (GIS: Ohashi et al. 1996). We applied standard screening procedures to the data and extracted the counts from a circular region centered on the target with a radius of 3 and 6 arcmin for SIS and GIS, respectively. We used standard blank sky observations to estimate the background. The SIS light curves of these 4 observations are shown in Figure 1. The count rate includes the background of $\sim$ 0.01 counts s^{-1}. The flux change between the observations 2 and 3 indicates variability on a time scale of about a day. The flux calculated from the spectrum decreased by a

factor 2 over two weeks. No evidence was found for time variability within each of the four observations; the maximum χ^2 probability of variability was less than 97 %.

We summed all photons detected with both SISs into a single spectrum for each observation, because the hardness ratio (defined as the ratio of counting rates at 1.5 – 7.5 keV to those at 0.7 – 1.5 keV) did not change significantly. Here we do not use the GIS data, since the efficiency of GISs in the low energy band (E $<$ 2 keV) is worse than that for SIS, and thus of less utility in a study of details of the spectral shape at low energies; furthermore, for this bright source, and a relatively simple model, with SISs alone, we probably reached the level where the statistical errors are comparable to the systematic errors. We first fitted such combined SIS spectra (one per observation) with a single power law with photoelectric absorption whose column density $N_{\rm H}$ was fixed at Galactic value, 1.73×10^{20} cm^{-2} (Elvis et al. 1989). However, this model did not represent any of the 4 spectra adequately; a power law fitting the data above 2 keV was too steep for the data below 2 keV. All the SIS data for these 4 observations showed such discrepancy that the reduced χ^2 ranged from 1.6 to 2.0 for more than 300 d.o.f. The single power law model is thus rejected with higher than 99 % confidence level.

A better fit was obtained using a broken power law model with Galactic absorption, where the spectrum is harder below the break. Even with this more complex model, we observe a clear spectral variability from one observation to another. As summarized in Table 1, the spectrum steepened as the flux decreased from (9.24 $\pm$ 0.05) to (4.21 $\pm$ 0.03)$\times 10^{-11}$ erg cm^{-2} sec^{-1} in 2 – 10 keV. The photon index (Γ_1) below the break energy (E_B) changed from 1.72 $\pm$ 0.08 to 1.89 $\pm$ 0.08 while the index (Γ_2) above E_B changed from 2.15 $\pm$ 0.02 to 2.46 $\pm$ 0.03. But the difference $\Gamma_2 - \Gamma_1$ was roughly constant, ~ 0.5, for all periods. Although we do not use GIS data for the above fits, the parameters derived here are consistent when we used both GIS2 and GIS3 data.

Figure 2 shows the correlation between the X–ray flux and the photon index. The maximum flux observed with *ASCA* was five times higher than the quiescent level observed with *Ginga* (Makino et al. 1991), and one fifth of the highest flux ever observed (Pian et al. 1998). As shown in Figure 2, the X–ray spectrum tends to steepen as the source gets fainter. This is a general feature of HBL spectra (see, e.g., Giommi et al. 1990). The spectral break around 2 keV was observed with both *ASCA* and *BeppoSAX* (Pian et al. 1998), while no spectral break was seen in the simultaneous *ROSAT* PSPC and *Ginga* observation, when the combined 0.1 – 20 keV spectrum was well-described by a power law with the photon index of 2.63 (Makino et al. 1991).

2.2. *EGRET*

We report here new *EGRET* results for Mrk 501, for which no *EGRET* detection has been reported previously. We have performed likelihood analysis (Mattox et al. 1996) of all viewing periods (VP) with exposure greater than 8×10^7 cm^2 s for γ-ray energies E > 100 MeV; the results are shown in Table 2. Contributions from diffuse high-latitude galactic emission and extragalactic emission (Sreekumar et al. 1998) were incorporated in the analysis. Note that for VP 519.0 the result is a 4.0 σ detection, barely meeting the acceptance criterion used in the construction of *EGRET* catalogs (Thompson et al. 1995).

At this point, considerable caution is required, because of the large size (~ 5 degrees) of the *EGRET* point spread function (PSF), and in this instance because of possible source confusion. Within 5 degrees of Mrk 501 are three flat spectrum radio quasars: (1) 3C 345 and (2) NRAO 512, neither of which have ever been convincingly detected by *EGRET* but which are otherwise similar to the highly variable *EGRET* -detected quasars; and (3) 4C +38.41, which has been detected several times by *EGRET* , and at times has been very bright. To verify that the source detected in VP 519.0 really was Mrk 501, an analysis was done for E > 500 MeV. Although the number of photons detected above 500 MeV is considerably smaller than above 100 MeV, the extent of the PSF for the higher-energy photons is reduced by a factor of about 6 in solid angle, enough to remove the possibility of confusion with the other nearby objects. The result of the E > 500 MeV analysis is a 5.2 σ detection, and source location contours (Figure 3) that clearly pinpoint Mrk 501 as the source of the γ-ray emission. The strong E > 500 MeV detection suggests a very hard spectrum, and indeed, spectral analysis gives a photon spectral index of 1.3 ± 0.5, one of the hardest spectra ever determined with *EGRET* .

The VP 516.5 & 519.0 observations listed in Table 2 have been examined for a possible time variability. A Kolmogorov-Smirnov (KS) test of the cumulative number of events (with E > 70 MeV) from the direction of Mrk 501 as a function of time has been performed (as described by Mattox et al. 1997a). For the 21 March – 3 April 1996 *EGRET* observation (which coincides with the *ASCA* observation described in §2.1), Kuiper's variant of the KS test (Press et al. 1992) indicates variability with 98.9 % confidence. This interval was therefore analyzed through a likelihood analysis of four equal length intervals with E $>$ 100 MeV. The light curve thus produced is shown in Figure 1. The second sub-interval, 24.96 – 28.17 March 1996, showed a detection significance of 3.5 σ, and a flux of (32 ± 13) $\times 10^{-8}$ cm^{-2}s^{-1}, E > 100 MeV. The spectral photon index was measured to be 1.6 ± 0.5 in the 30 MeV – 10 GeV energy range during the 24.96 – 28.17 March 1996 sub-interval. A χ^2 test of variability using the fluxes of these four intervals indicates variability with 88 % confidence. From Figure 1, a correlation with the TeV flux appears plausible, but the

EGRET statistics are too sparse for a definitive evaluation. For the 23 April 1996 – 7 May 1996 exposure, Kuiper's variant of the KS test indicates variability with 95 % confidence. Higher flux is indicated between 23.88 and 29.13 April 1996 and 4.19 and 7.44 May 1996. For the 4 – 15 April 1997 exposure, a likelihood analysis finds a 1.5 σ indication of E > 100 MeV flux. During this interval, Mrk 501 was observed to flare in the TeV and hard X–ray bands (Catanese et al. 1997; Aharonian et al. 1997; Pian et al. 1998).

For VP 516.5 and VP 617.8, there are not enough photons above 500 MeV to enable an analysis similar to that done for VP 519.0 above 500 MeV. For VP 516.5, the time proximity to the rather strong emission in VP 519.0 suggests that Mrk 501 is probably the source of the 2.1 σ detection, and particularly the 3.5 σ detection in the 3.2-day subinterval of the multiwavelength campaign, especially in view of the TeV activity during that time.

The one-year interval between VP 519.0 and VP 617.8 prevents any similar conclusion based on the *EGRET* data alone; however, the strong TeV activity during VP 617.8 again suggest that Mrk 501 is the source of γ–ray radiation possibly detected by *EGRET* at that time.

2.3. TeV observations

Mrk 501 was observed at E > 350 GeV with the *Whipple Atmospheric Cherenkov Imaging Telescope* (Cawley & Weekes 1995) from 1996 March 17 to 30 as a part of the multiband campaign. The data for the nights of March 21 and 22 were discarded due to poor weather conditions. The resulting data set comprises 17.5 hours of good weather observations. The data were analyzed with the Tracking analysis using the γ–ray selection criteria optimized on Crab Nebula data (see, e.g., Quinn et al. 1996). The resulting light curve is shown in Figure 1. The average emission level for the observation period is 0.20 $\pm$ 0.03 photons min^{-1}, approximately 15 % that of the corresponding rate from the Crab Nebula. This is almost double the average flux level observed from Mrk 501 in 1995 (Quinn et al. 1996). The flux appears to be highest on the first night of observation (0.46 $\pm$ 0.10 photons min^{-1}), and then decreases over a period of a couple of days to a relatively constant level of 0.15 $\pm$ 0.03 photons min^{-1}. A χ^2 analysis for constant emission produces a χ^2 / d.o.f of 21.5 / 11, which indicates variability at the 97 % level (a 2.3 σ effect). The χ^2 test was also applied to each night's data to search for evidence of variability within a night — none was found.

According to Petry et al. (1997; see also Bradbury et al. 1997), *HEGRA* also observed Mrk 501 from March 28 to August 1996, partially overlapping our observation. The energy

threshold was 1.5 TeV. The photon index of combined spectrum during this 5 months was measured to be 2.5 ± 0.4 (total error) and the average flux was consistent with that of *Whipple* measured during our campaign in March 1996.

2.4. Optical observations

A few optical observations were carried out using the 70 cm telescope of the Landessternwarte in Heidelberg. Poor weather prohibited strictly simultaneous observations for most of the campaign. It was possible, nevertheless, to obtain a few measurements on March 26 and 27, 1996. Three observations in R-band were taken in both nights, separated by about one hour. Since no variability was found within either of the nights within the photometric accuracy of ~ 1.8 %, the three frames were co-added and an average flux for each of the nights was derived. The observed magnitude at 650 nm was $m_R = 11.80 \pm 0.02$ for March 26 and $m_R = 11.72 \pm 0.02$ for March 27. The probability of variability in the optical band within the two nights is only 2.3 σ, and hence not significant. The average brightness in each night is about 30 % lower than the average brightness in the R-band measurements from the NED data base. Since the absolute fluxes in any optical band depends on the correction for the contribution of the host galaxy and a bit on the effective transmission of standard filters and CCD response, it is not possible to judge whether this difference is due to the source activity or systematic differences.

3. Multiband Spectrum

The multiband spectra of Mrk 501 taken during our campaign and at other times are shown in Figure 4. Open circles show the *ASCA*, *EGRET* , *Whipple* and optical data for March 25 – 28 in 1996, when *EGRET* detected the emission E > 100 MeV from Mrk 501 for the first time at 3.5 σ level. The *ASCA* points are determined from a combined fit of data taken during observation 2 and 3. The X–ray flux in the 2 – 10 keV band was 6.0×10^{-11} erg cm^{-2} s^{-1}. The TeV count rates observed with *Whipple* are converted to integral fluxes by scaling them as a multiple of Crab Nebula count rate with assumption that the photon index is as same as that of Crab, 2.5 (Hillas et al. 1998). The TeV flux plotted in Figure 4 is $(1.23 \pm 0.6)\times10^{-11}$ photons cm^{-2} s^{-1}, consistent with the flux in 1995, $(0.8 \pm 0.1)\times10^{-11}$ photons cm^{-2} s^{-1} (Quinn et al. 1996). The optical point is an average value of March 26 and 27, converted to the energy flux of $(5.40 \pm 0.07)\times10^{-11}$ erg cm^{-2} s^{-1}.

In order to know the change of the multifrequency spectra for various phases of source

activity, we also plot in Figure 4 the spectra for the pre – 1995 quiescent state, and the April 1997 flare. Although the X–ray flux observed with *ASCA* was decreasing over a 2-week period, the long-term changes of the X–ray spectra from 1991 (*Ginga*) to 1997 (*BeppoSAX*) suggest that our March 1996 multiwavelength campaign was conducted in the transition phase from the quiescent to the high state. Since a transition of the states in blazars is certainly not smooth or monotonous, the fact that the X–ray flux observed with *ASCA* was decreasing is essentially irrelevant for this interpretation.

The differences in the spectral indices observed with *ASCA* ($\Gamma_2 - \Gamma_1$; see Table 1) show roughly constant value of ~ 0.5, which is expected from the synchrotron cooling process (e.g., Sikora, Begelman & Rees 1994; Mastichiadis & Kirk 1997). Together with the fact that the peak of the synchrotron emission ordinarily exists near the UV band in the quiescent state (George et al. 1988), the spectral break around 2 keV observed with *ASCA* , when the source was in the 'intermediate' state, is considered to be the peak of the synchrotron emission. The location of this break increased to ~ 100 keV when the source was in the high state (Pian et al. 1998). We compare the X–ray and TeV fluxes between three multiwavelength observations: March 1996, April 7 and April 16, 1997. Compared with that in March 1996, the 2 – 10 keV flux was higher by a factor of 3.6 on April 7 1997, and a factor of 8.9 on April 16 1997. The simultaneous increase in the *Whipple* flux above 350 GeV for these two dates was by factors of 4.9 and 33 respectively. We discuss the amplitude for the correlated variation of the keV and TeV band in the next section.

4. Discussion

During our campaign in March 1996, a variability of about 30 % in the X-ray flux was observed on time scale of a day from Mrk 501. Assuming that the radiation is isotropic and all photons are created in the same region of the size implied by the variability time scale t_{var}, the optical depth to pair production for TeV and keV photons is estimated as $\tau \gtrsim 30$ (e.g., Mattox et al. 1997a), where t_{var} (as measured in the observer's frame) is assumed to be 10^5 sec. To avoid absorption of γ–rays due to pair production, current models of blazars assume that the radiation is Doppler boosted (e.g., Maraschi et al. 1992). We can limit the beaming factor to $\delta \gtrsim 1.9$ (assuming $H_0 = 75$ km s^{-1} Mpc^{-1}). However, a stronger limit should be imposed if there were more rapid flux changes which we could not detect because of our sampling. For instance, during the low state in 1986, an X-ray variability on a time scale of a few hours was observed from Mrk 501 by *EXOSAT* (Giommi et al. 1990). Quinn et al. (1998) also reported variability with a doubling time of 2.5 hours in the TeV band during one flare in June 1997. Furthermore, there exists an evidence of correlated

variability in U-band and TeV band, during the flare in April 1997 (Catanese et al. 1997). In this case, we can strengthen the limit for beaming factor to $\delta \gtrsim 6.4$ for t_{var} of 10^4 sec.

We apply a one-zone, homogeneous SSC model to the March 1996 multiband data, generally following the prescriptions of Inoue & Takahara (1996). A spherical geometry is adopted, with R being the radius of the emission region. An injection of a power-law energy distribution of electrons up to a certain maximum energy (as expected from shock acceleration) into the radiating region should yield a steady-state electron distribution with a break in its index at a characteristic energy, determined by the balance between radiative cooling and advective escape and/or adiabatic energy loss. (e.g., Sikora, Begelman & Rees 1994; Mastichiadis & Kirk 1997). The resulting synchrotron emission spectrum should reflect this broken power-law form, with the electron index p related to the spectral energy index of the emission α by $\alpha = (p-1)/2$. What the observed multiband spectrum (Figure 4) actually suggests is the presence of two breaks in the synchrotron component; one in the IR to optical region, and the second in the X–ray band, both with the spectral index changes of ~ 0.5. Moreover, we were unable to adequately fit the whole spectrum including the γ–ray band with a model utilizing an electron distribution with only one break and a maximum energy cutoff. We therefore choose to employ a double broken power-law form for the electron distribution $N(\gamma)$, in which $N(\gamma) \propto \gamma^{-s}$, $\propto \gamma^{-s-1}$ and $\propto \gamma^{-s-2}$ in the energy ranges $\gamma \lesssim \gamma_{b1}$, $\gamma_{b1} \lesssim \gamma \lesssim \gamma_{b2}$ and $\gamma_{b2} \lesssim \gamma \lesssim \gamma_{max}$, respectively. The injection index s is taken to be $s = 2$, and we treat the two break Lorentz factors γ_{b1}, γ_{b2} and the maximum Lorentz factor γ_{max} as parameters. (The particular form employed in the calculations below, $N(\gamma) \propto \gamma^{-s}(1+\gamma/\gamma_{b1})^{-1}(1+\gamma/\gamma_{b2})^{-1}$, was chosen simply for convenience; using sharp breaks instead produces only small changes in the resulting spectrum.) Such a second break (or equivalently, a broad cutoff) in the distribution may effectively result from incorporating a more realistic geometry and/or detailed kinetic evolution of the particle distribution in the downstream region of the shock front (see, e.g., the discussion in Kirk, Rieger & Mastichiadis 1998). However, a deeper inquiry into this aspect is beyond the scope of this paper; here it is only introduced in order to provide a better description of the data.

Synchrotron emission including self-absorption is calculated using the standard spherical solution to the radiative transfer equation,

$$L_{sync}(\nu) = 4\pi^2 R^2 \frac{j_\nu}{\alpha_\nu}\left(1 - \frac{2}{{\tau_\nu}^2}[1 - e^{-\tau_\nu}(\tau_\nu + 1)]\right) \qquad (1)$$

where j_ν and α_ν are respectively the emission and absorption coefficients for synchrotron radiation (e.g., Blumenthal & Gould 1970; Gould 1979; Bloom & Marscher 1996). τ_ν is the optical depth in the blob along the line of sight and expressed as $\tau_\nu = 2\alpha_\nu R$. The electron pitch angle with respect to the magnetic field is set to $\theta = \pi/2$.

We calculate the inverse Compton emission incorporating the effects of cross section reduction in the Klein-Nishina regime. The differential photon production rate $q(\epsilon)$ is

$$q(\epsilon) = \int d\epsilon_0 n(\epsilon_0) \int d\gamma N(\gamma) C(\epsilon, \gamma, \epsilon_0) \tag{2}$$

where ϵ_0 and ϵ are respectively the soft photon energy and the scattered photon energy in units of $m_e c^2$, $n(\epsilon_0)$ is the number density of soft photons per energy interval, and $C(\epsilon, \gamma, \epsilon_0)$ is the Compton kernel of Jones (1968). To be exact, $n(\epsilon_0)$ varies depending on the position in the emission blob and we have to take this effect into account. Approximately, we calculated $n(\epsilon_0)$ at the center of the blob with the correction factor of $C_{corr} = 0.75$ (Gould 1979). Thus we have

$$n(\epsilon_0) = \frac{4\pi}{hc\epsilon_0} C_{corr} \frac{j_\nu}{\alpha_\nu} (1 - e^{-\alpha_\nu R}) \tag{3}$$

where h is the Planck constant. The convolution in equation (2) is performed under the condition

$$\epsilon_0 \leq \epsilon \leq \gamma \frac{4\epsilon_0 \gamma}{1 + 4\epsilon_0 \gamma} \tag{4}$$

from the kinematics of electron-photon scattering.

We applied this model to the observed spectrum of Mrk 501. To approximate the values for magnetic field and beaming factor, we first place constraints on the allowed parameter space similar to Bednarek & Protheroe (1997), calculated for the case of Mrk 421. In the following prescriptions, we basically assume the parameter space for the March 1996 data. However, because of the lack of the information in the hard X-ray band and the high energy tail of the TeV spectrum during this campaign, we also use the non-contemporaneous data sets for the calculation.

Since the *Ginga* data in the quiescent state shows no spectral cut off below 20 keV (Figure 4), it is probable that the synchrotron spectrum in March 1996 also extends above 20 keV. We assume here the maximum synchrotron energy at 50 keV. We thus obtain $\gamma_{max} = 3.2{\times}10^6\ B^{-0.5}\ \delta^{-0.5}$. The Compton-scattered spectrum extending to higher than 10 TeV (Aharonian et al. 1997) gives us the limitation of $\gamma_{max}\ m_e c^2 \geq 10\ \mathrm{TeV}/\delta$. Using both equations, we can limit the magnetic field to $B \leq 2.6{\times}10^{-2}\ \delta$ Gauss. This limit is represented by line (I) in Figure 5.

The second constraint is derived using the ratio of the synchrotron and Compton luminosities. Here we can use a relation for the Thomson regime since the Compton luminosity is well approximated as that for the *EGRET* range and the high-energy γ-ray spectrum shows no sign of Klein-Nishina cutoff in the MeV – GeV band (Figure 4). Thus the energy density of the synchrotron radiation u_{sync} is related to the magnetic field density

u_B as $u_B = u_{sync}\,(L_{sync}/L_{SSC})$, where L_{sync} and L_{SSC} is the observed synchrotron/Compton luminosity. Since u_{sync} is represented as

$$u_{sync} = \frac{L_{sync}}{4\pi R^2 c\delta^4} \tag{5}$$

we have the relation

$$u_B = \frac{{d_L}^2}{R^2 c\delta^4}\frac{{l_{sync}}^2}{l_{SSC}} \tag{6}$$

where d_L is the luminosity distance, l_{sync} and l_{SSC} are energy flux in observer's frame. From Figure 4, we can approximate l_{sync} and $l_{SSC} \sim 10^{-10}$ erg cm^{-2} s^{-1}. The upper limit for R is also given as

$$R \leq ct_{var}\delta \tag{7}$$

where t_{var} is the minimum variability time scale in the observer's frame. Using equation (6) and (7), with t_{var} expressed in seconds, we obtain $B \geq 4{\times}10^6\ t_{var}^{-1}\ \delta^{-3}$ Gauss. This limit is represented by line (II) in Figure 5.

The third constraint is derived from the evaluation of a variability time scale and synchrotron cooling time scale (t_{sync}). Although the minimum variability time scale must be determined by the balance between radiative cooling and adiabatic energy loss or advective escape (e.g., Sikora, Begelman & Rees 1994; Mastichiadis & Kirk 1997), the synchrotron emission can be one of the most dominant cooling processes; the X-ray spectrum of Mrk 501 which tends to steepen as the source gets fainter supports this assumption (see Figure 2). For the electrons of large γ ($\gamma \geq \gamma_{b1}$), t_{sync} is smaller than the source crossing time scale R/c. Combining this with equation (7), we obtain $t_{var}\delta \geq t_{sync}$. Since t_{sync} is represented as

$$t_{sync} = \frac{3m_e c}{4u_B\sigma_T\gamma} \tag{8}$$

where σ_T is the Thomson cross section, it becomes minimum at $\gamma = \gamma_{max}$. The lower limit for B is thus calculated as $B \geq 3.9{\times}10\ t_{var}^{-2/3}\ \delta^{-1/3}$ Gauss. This limit is represented by line (III) in Figure 5.

The final constraint is that from the evaluation of the variability time scale and Compton cooling time scale (t_{SSC}). Even for the creation of TeV photons, scatterings in the Thomson regime can be dominant if $\gamma_{max}h\nu < m_e c^2\delta$ and $\gamma_{max}^2 h\nu > 1$ TeV are satisfied at the same time, where $h\nu$ is the soft photon energy in the observer's frame. These inequalities have a self-consistent solution for $h\nu < \delta^2/4$ eV, under the condition of $B < 5\delta$ Gauss. We then approximate t_{SSC} using equation (8), replacing the magnetic field density by the synchrotron photon density. To estimate the value of u_{sync}, $L_{sync} \sim 10^{45}$ erg s^{-1} is used here. Thus t_{SSC} at $\gamma = \gamma_{max}$ is calculated as $3{\times}10^{-12}\ t_{var}^2\ B^{0.5}\delta^{6.5}$, where we assume

R as $ct_{var}\delta$, rather than using inequality (7). This is not true in the strict sense, although it is plausible if t_{SSC} at $\gamma = \gamma_{max}$ is much shorter than t_{var} δ. The previous discussion for $t_{var}\delta \geq t_{sync}$ supports our assumption if $u_B \sim u_{sync}$. The magnetic field is then calculated to be $B \leq 9{\times}10^{22}\ t_{var}^{-2}\ \delta^{-11}$ Gauss. This limit is represented by line (IV) in Figure 5.

In Figure 5, we show the allowed values of B as a function of δ for the case of Mrk 501 data sets. These four limits are derived for t_{var} of 10^5 sec, which is observed with *ASCA* in March 1996. We also calculate the limits that corresponds to the minimum time scale t_{var} of 10^4 sec, for more rapid flux changes that we could not detect because of our sampling. The input parameters for our model are determined at the center of the overlapped region for those different time scales : $B = 0.2$ Gauss, $\delta = 15$ and $R = 4.5 \times 10^{15}$ cm. The electron distribution is then fixed as: $\gamma_{min} = 1.0$, $\gamma_{b1} = 1.2 \times 10^4$, $\gamma_{b2} = 3.7 \times 10^5$ and $\gamma_{max} = 1.8 \times 10^6$. As shown in Figure 4, the whole spectrum is adequately represented, except for the IR/optical feature near 10^{14} Hz and a discrepancy in the TeV spectrum. One can also see the discrepancy in the radio band, but this can be an effect of at least a part of the emission arising at a larger distance than the location of the keV/TeV emitting region. The one-zone models cannot account for the low-energy emission, which is thought to be produced in a much larger region of the source (e.g., Marscher et al. 1980; see also Pian et al. 1998). However, investigation of this low-energy discrepancy is beyond the scope of this paper; in the following, we concentrate on the discrepancy in the higher energy band where the one-zone models are thought to be a reasonable approximation to account for the power output of blazars.

The predicted photon index in the *HEGRA* band is 3.8, while the observed value is 2.5 $\pm$ 0.4 (Petry et al. 1997; Bradbury et al. 1997). The photon index in the *EGRET* energy range (30 MeV – 10 GeV) is predicted to be 1.8 which is consistent with the observed value of 1.6 $\pm$ 0.5. The rest–frame luminosity is also calculated to be $L'_{sync} = 2.2 \times 10^{40}$ erg s^{-1} and $L'_{SSC} = 1.8 \times 10^{40}$ erg s^{-1}. From integration of $\gamma N(\gamma)$, the energy density of relativistic electrons in the source frame is estimated to be 0.16 erg cm^{-3} and Compton optical depth is $\tau_c = 6.3 \times 10^{-5}$.

It is worthwhile to compare the overall spectrum, and the parameters derived by us to those obtained for Mrk 421 (see, e.g., Takahashi et al. 1996a). Observationally, the spectrum of Mrk 421 also shows a spectral break around 1 keV, but its energy does *not* seem to vary more than a factor of a few when the source enters a flare state, while Mrk 501 shows a change of a factor of ~ 100. Our modelling indicates that the derived magnetic field B is comparable between the two sources, on the order of 0.2 Gauss, but the main difference appears to be the energy of electrons radiating at the peak of the synchrotron component during the flare, γ_{max}, which for Mrk 421 is a few $\times$ 10^5 to 10^6, while for the flare of Mrk

501, it is larger, several $\times 10^6$ or greater (e.g., Inoue & Takahara 1996; Pian et al. 1998; see also below). While for Mrk 421, an independent verification of these parameters exists via the comparison of the Klein-Nishina limit to the implications of the spectral variability observed in X–rays (e.g., Mastichiadis & Kirk 1997; Bednarek & Protheroe 1997), we do not have a well-sampled X–ray light curve for Mrk 501, and thus cannot make such a comparison here.

In any case, those large differences indicate that the overall electromagnetic spectra of HBLs are qualitatively similar, but peaking at different energies, which is likely to be a result of different energy distribution of radiating electrons. Kubo et al. (1998) found that B is similar over a large range of blazar classes, and the difference of the overall spectra – where the blazars associated with quasars (showing emission lines) have synchrotron components peaking in the infrared, as opposed to HBLs, where these peaks are in the X–ray regime – can be also explained by lower γ_{max} in quasar-type blazars than in HBLs. However, it is not possible as yet to determine if this is intrinsic, i.e. related to different conditions for the particle acceleration process, or if some external conditions (such as the strong diffuse radiation field) play an important role in the particle population inferred from the observations.

We next investigate whether the one-zone SSC model might be helpful to understand the large flare observed in April 1997. Inspection of Figure 4 suggests that two different components probably contribute to the synchrotron spectrum, one a steady component, and another, variable, responsible for the sudden increase of the highly energetic electrons, when the source goes into the flare state. We set γ_{max} to 5.5×10^6 for the April 7 data and 7.0×10^6 for the April 16 data. The parameters such as region size, magnetic field, and beaming factor are the same as that for March 1996. The normalization was determined from the synchrotron spectra obtained during the *BeppoSAX* observations (Pian et al. 1998). For these flare data, a single break population of electrons is adequate to account for the multiband spectrum ($\gamma_{b1} \sim \gamma_{b2}$).

We first assumed that the newly injected electrons scatter only the photons emitted by the electron population associated with the flare. However, the calculated flare amplitude of the TeV flux was substantially lower than that observed. We next assumed that there exists a steady population of synchrotron photons, with the same level as that in 1996, and those are scattered by the flare electron population. In this case, the flare amplitude of the TeV flux is quite well reproduced as shown in Figure 4. The photon index in the *HEGRA* region is predicted to be 2.6 for April 7 1997, comparable with the observational data of $2.49 \pm 0.11 \pm 0.25$ (Aharonian et al. 1997). This result is consistent with Pian et al. (1998), where the scattering of the steady component by the flare electron population is necessary

to account for the flare amplitude of the TeV flux. This may imply that the steady and the flare components arise from close parts of the jet, having some interaction with each other. Unfortunately, the observed data during the flare are too sparse to discriminate whether the two emission components originate in the same region or different regions of the jet. More precise observations in various energy bands (and, in particular, better sampling) are necessary to further understand this problem.

The relatively flat shape of the spectrum observed with *HEGRA* in March 1996 is discrepant with our one-zone model. We investigated two possible causes of this discrepancy. The first is the external soft photons from the host galaxy or obscuring torus and the other is the multiple Comptonization. The integration of the stellar light from the galaxy can be the origin of the IR/optical feature present around 10^{14} Hz (see Figure 4; Falomo et al. 1993). These photons are distributed isotropically in the observer's frame and are injected externally into the emission region. The IR photons are important since they can be scattered to TeV energies ($\gamma_{max} \sim 10^6$) without entering the Klein-Nishina regime. Additionally, Comptonization of such external photons can be more effective than SSC, because of the anisotropy of injected photons in the frame of the jet (Sikora et al. 1994; Dermer 1995; Dermer et al. 1997). To account for the flat TeV spectrum with such external radiation, the observed external Compton luminosity (L_{ext}) must be at least comparable with the synchrotron luminosity (L_{sync}). This means that the energy densities of magnetic field and external photons have the relation $u_{ext} \sim u'_{ext}/\delta^2 \gtrsim u_B/\delta^4$, where u_{ext} is the density of external photons in the observer's frame and u'_{ext} in the jet frame. For our model of $B = 0.2$ Gauss and $\delta = 15$, we obtain the constraint of $u_{ext} \gtrsim 10^{-8}$ erg cm^{-3}. The typical values for the total luminosity of the galaxy $L_{gal} = 10^{44}$ erg s^{-1} and effective radius $R_{eff} =$ 1 kpc (e.g., Binney & Tremaine 1987) give the energy density of $u_{ext} \sim 3 \times 10^{-11}$ erg cm^{-3} — much smaller than the lower limit given above and thus the galactic IR photons aren't expected to affect the TeV spectrum.

However, if the IR photons arise in a region comparable to a parsec-scale torus, postulated to exist in Seyfert galaxies (e.g., Antonucci & Miller 1985; Krolik & Begelman 1986) — then, such a photon field may be important (e.g., Sikora et al. 1994). These photons can be emitted from the dust around the nucleus, but may be hidden by the strong jet emission in the observer's frame; in fact, our spectrum (see Figure 4) does not exclude such emission. We can easily predict that if the total luminosity of such IR photons exceeds $L_{dust} \gtrsim 10^{43}$ erg s^{-1}, it can contribute sufficient seed photons that subsequently would be Comptonized to dominate the TeV spectrum. The precise (sub-arcsec) IR/optical imaging of Mrk 501 should limit the spatial extent of the 'IR–bump' mentioned above.

The second possible cause of the TeV spectral discrepancy is the contribution of

photons produced by multiple Compton scattering (e.g., Band et al. 1985, 1986; Bloom & Marscher 1996). In considering the second-order scattering, the same formula (2) is used, except that the incident photons are now the first-order inverse Compton photon density (Bloom & Marscher 1996). Our calculation shows the contribution from multiple Compton scattering is greatly suppressed due to the Klein-Nishina effect. The flux ratio for Comptonization of first and second order is $f_{2nd}/f_{1st} \lesssim 10^{-3}$ at 1 TeV. Thus, the second order SSC process does not make a significant contribution to the spectrum, and we are unable to explain the relatively flat TeV spectrum in March 1996.

A beaming factor much larger than 10 could also make TeV spectrum flatter. However, our previous calculation shows that at $\delta \gtrsim 40$, Compton cooling time for highly energetic electrons becomes larger than the source crossing time scale R/c and thus no clear break should appear in the electron population. Also, a beaming factor much larger than 10 (e.g., $\delta \gtrsim 100$) doesn't reproduce the GeV/TeV flux ratio of $f_{EGRET}/f_{Whipple} \sim 10$, but makes both fluxes comparable because most of the scattering will take place in the Thomson regime.

Although the boundary for the allowed parameter space could be changed if variability on shorter time scales is found (see Figure 5), a more tightly constrained TeV spectral index (through better statistics and less systematic error) will be of great value to make further progress on modelling of this source. Together with more refined SSC models such as Marscher (1980) and Ghisellini & Maraschi (1989), we have shown that an exact evaluation of Comptonized emission from external IR photons, such as dust emission around the nuclei and accretion disk photons, may be useful for the understanding of the origin of the flat TeV spectrum. Our model here is constructed with no time dependence. To be exact, this model should be expanded to include the full time dependent evolution of the electron and photon spectra (e.g., Mastichiadis & Kirk 1997). The time dependent treatment for Mrk 501 flare will be discussed elsewhere.

5. Conclusion

We have conducted a multiwavelength campaign for the TeV blazar Mrk 501 in March 1996. In the *EGRET* data, we found 3.5 σ detection (E > 100 MeV) of high-energy γ-rays. Higher flux was also observed in April/May 1996, with 4.0 σ significance for E > 100 MeV, and 5.2 σ significance for E > 500 MeV. The maximum flux observed with *ASCA* was 5 times higher than the quiescent level and gradually decreased by a factor of 2 as the spectrum steepened. The spectra obtained with *ASCA* show a 'break' around 2 keV, which is interpreted as the peak of the synchrotron emission. Comparing our results with

the observations in April 1997, there were notable changes in overall spectra, such as a 2 decade shift of the peak frequency of the synchrotron component, a change of peak flux in the keV region by a factor of 9, and a flux change in the TeV region by a factor of 33. To investigate a correlated variation of spectra in the keV and TeV region, we applied a one-zone, homogeneous SSC model with an electron distribution having two break points. The allowed parameter space (B, δ) was systematically investigated to obtain values for the model parameters. The spectrum in March 1996 was consistent with parameters γ_{max} = 1.8 $\times$ 10^6, B = 0.2 Gauss, δ = 15, and R = 4.5 $\times 10^{15}$ cm. The correlation of the keV/TeV flare amplitudes in April 1997 was also reproduced with the assumption that an additional electron population, with higher maximum energies ($\gamma_{max} \sim 6 \times 10^6$) was newly injected and scattered the photons emitted from the steady component, assumed to be the same level as that in 1996. We found that the scattering of the synchrotron photons emitted from only the flare electron population is inadequate in our model. The flat TeV spectrum observed with *HEGRA* in March 1996 is discrepant with our model. We considered the contribution from the galactic IR photons, and higher order Comptonization, and found that neither could make the TeV spectrum flatter. A possible contribution from a parsec-scale torus, postulated to exist in Seyfert galaxies, was also investigated. We need better quality data, especially in the hard X–ray and γ–ray regimes, to better understand the emission mechanism. Observations with a next generation of satellites, featuring improved sensitivity at hard X–ray/γ–ray energies, such as *Astro – E* and *GLAST* , are expected to bring valuable information.

This research has made use of the NASA/IPAC Extragalactic Database (NED) which is operated by the JET Propulsion Laboratory, Caltech, under contact with the national Aeronautics and Space Administration, and made use of data from the University of Michigan Radio Astronomy Observatory which is supported by the National Science Foundation and by funds from the University of Michigan. We would like to thank Dr. A. P. Marscher, Dr. T. C. Weekes and an anonymous referee for their constructive comments and discussions. We also thank Dr. M. Tashiro and Dr. T. Mihara for communication of the *Ginga* data in 1991. J. R. Mattox acknowledges support from NASA grant NAC 5-3384.

REFERENCES

Antonucci, R., & Miller, J. 1985, ApJ, 297, 621

Aharonian, F., et al. 1997, A&A, 327, L5

Band, D. L., & Grindlay, J. E. 1985, ApJ, 298, 128

Band, D. L., & Grindlay, J. E. 1986, ApJ, 308, 576

Bednarek, W., & Protheroe, R. J. 1997, MNRAS, 292, 646

Binney, J., & Tremaine, S. 1987, Galactic Dynamics, Princeton University Press

Bloom, S. D., & Marscher, A. P. 1996, ApJ, 461, 657

Blumenthal, G. R., & Gould, R. J. 1970, Rev. Mod. Phys., 42, 237

Bradbury, S. M. 1997, A&A, 320, L5

Buckley, J. H., et al. 1996, ApJ, 472, L9

Burke, B. E., et al. 1991, IEEE Trans. ED-38, 1069

Catanese, M., et al. 1997, ApJ, 487, L143

Catanese, M., et al. 1998, ApJ, in press

Cawley, M. F., & Weekes, T. C. 1995, Exp. Astron., 6, 7

Dermer, C. D., & Schlickeiser, R. 1993, ApJ, 416, 458

Dermer, C. D. 1995, ApJ, 446, L63

Dermer, C. D., Stauner, S. J., & Schlickeiser, R. 1997, ApJS, 109, 103

Elvis, M., et al. 1989, AJ, 97(3), 777

Falomo, R., et al. 1993, AJ, 106(1), 11

Fichtel, C. E., et al. 1994, ApJS, 94, 551

Gaidos, J. A., et al. 1996, Nature, 383, 319

George, I. M., Warrick, R. S., & Bromage, G. E. 1988, MNRAS, 232, 793

Ghisellini, G., & Maraschi, L. 1989, ApJ, 340, 181

Giommi, P., et al. 1990, ApJ, 356, 432

Gould, R. J., et al. 1979, A&A, 76, 306

Hillas, A. M. 1998, in preparation

Inoue, S., & Takahara, F. 1996, ApJ, 463, 555

Jones, F. C. 1968, Phys. Rev., 167, 1159

Jones, T. W., O'Dell, S. L., & Stein, W. A. 1974, ApJ, 188, 353

Kirk, J. G., Rieger, F. M. & Mastichiadis, A. 1998, A&A, in press

Kőnigl, A. 1981, ApJ, 243, 700

Kubo, H., et al. 1998, ApJ, in press

Krolik, J., & Begelman, M. 1986, ApJ, 308, L55

Macomb, D., et al. 1995, ApJ, 449, L99

Makino, F., Fink, H. H., & Clavel, J. 1992, in Frontiers of X–ray Astronomy, Universal Academy Press, Y.Tanaka & K.Koyama, 543

Marscher, A. P. 1980, ApJ, 235, 386

Marscher, A. P., & Gear, W. K. 1985, ApJ, 298, 114

Marscher, A. P. & Travis, J. P. 1996, A&AS, 120, 537

Maraschi, L., Ghisellini, G., & Celotti, A. 1992, ApJ, 397, L5

Mastichiadis, A., & Kirk, J. G. 1997, A&A, 320, 19

Mattox, J. R., et al. 1993, ApJ, 410, 609

Mattox, J. R., et al. 1996, ApJ, 461, 396

Mattox, J. R., et al. 1997a, ApJ, 476, 692

Mattox, J. R., et al. 1997b, ApJ, 481, 95

Mukherjee, R., et al. 1997, ApJ, 490, 116

Ohashi, T., et al. 1996, PASJ, 48, 157

Petry, D., et al. 1996, A&A, 311, L13

Petry, D., 1997, PhD thesis, Max-Planck-Institute for Physics, Munich, report MPI-PhE/97-27

Pian, E., et al. 1998, ApJ, 492, L17

Press, W. H., et al. 1992, Numerical Recipes in C (Cambridge : Cambridge Univ.Press)

Punch, M., et al. 1992, Nature, 358, 477

Quinn, J., et al. 1996, ApJ, 456, L83

Quinn, J., et al. 1998, in preparation

Sreekumar, P., et al. 1998, ApJ, 494, 523

Ulrich, M. –H., Maraschi, L., & Urry, C. M. 1997, ARAA, 35, 445

Sikora, M., Begelman, M. C., & Rees, M. J. 1994, ApJ, 421, 153

Takahashi, T., et al. 1996a, ApJ, 470, L89

Takahashi, T., et al. 1996b, Mem. Soc. Astron. Ital., 67, 533

Thompson, D. J., et al. 1993, ApJS, 86, 629

Thompson, D. J., et al. 1995, ApJS, 101, 259

von Montigny, C., et al. 1995, ApJ, 440, 525

Weekes, T. C., et al. 1996, A&AS, 120, 603

This preprint was prepared with the AAS LaTeX macros v4.0.

Table 1. Fit result of *ASCA* spectrum

Obs.ID	time(UT in 1996)	Γ_1[a]	E_B[a]	Γ_2[a]	Flux[b]	$\Gamma_2-\Gamma_1$	χ^2 / (d.o.f)
1	Mar 21.26–21.50	1.72±0.02	1.72±0.08	2.15±0.02	9.24±0.05	0.43±0.03	1.00(379)
2	Mar 26.12–26.42	1.77±0.03	1.67±0.08	2.22±0.02	7.03±0.04	0.45±0.04	0.92(360)
3	Mar 27.70–27.95	1.89±0.03	1.67±0.07	2.35±0.02	5.20±0.03	0.46±0.04	1.04(329)
4	Apr 2.69–2.93	1.89±0.03	1.65±0.07	2.46±0.03	4.21±0.03	0.57±0.04	1.04(313)

[a] Fit model is broken power law with Galactic absorption. Γ_1 and Γ_2 are photon indices in lower and higher energy band, respectively. E_B is break energy in keV. SIS0 and SIS1 data are combined.

[b] 2–10 keV flux in units of 10^{-11}erg cm^{-2} s^{-1}.

All errors are 1 σ.

Table 2. *EGRET* results for Mrk 501

EGRET VP[a]	Interval	Aspect[b]	Exposure[c]	Significance (σ)	Flux[d]
9.5	12-Sep-1991 — 19-Sep-1991	3.3°	2.28	0.5	<11
201.0	17-Nov-1992 — 24-Nov-1992	2.5°	1.12	1.7	9±6
202.0	24-Nov-1992 — 01-Dec-1992	5.8°	1.06	1.1	8±7
516.5	21-Mar-1996 — 03-Apr-1996	3.1°	1.47	2.1	10±5
	(25-Mar-1996 — 28-Mar-1996)		0.46	3.5	32±13
519.0	23-Apr-1996 — 07-May-1996	1.2°	2.10	4.0	18±5
	(E>500 MeV)		2.97	5.2	[e]6±2
617.8	04-Apr-1997 — 15-Apr-1997	3.0°	0.82	1.5	9±7

[a] *EGRET* Viewing Period.

[b] Angle between the source and the *EGRET* instrument axis.

[c] exposure in unit of 10^8 cm^2 s.

[d] Flux (E>100 MeV) in units of 10^{-8} cm^{-2}s^{-1}. All errors are 1 σ.

[e] Flux (E>500 MeV) in units of 10^{-8} cm^{-2}s^{-1}. The error is 1 σ.

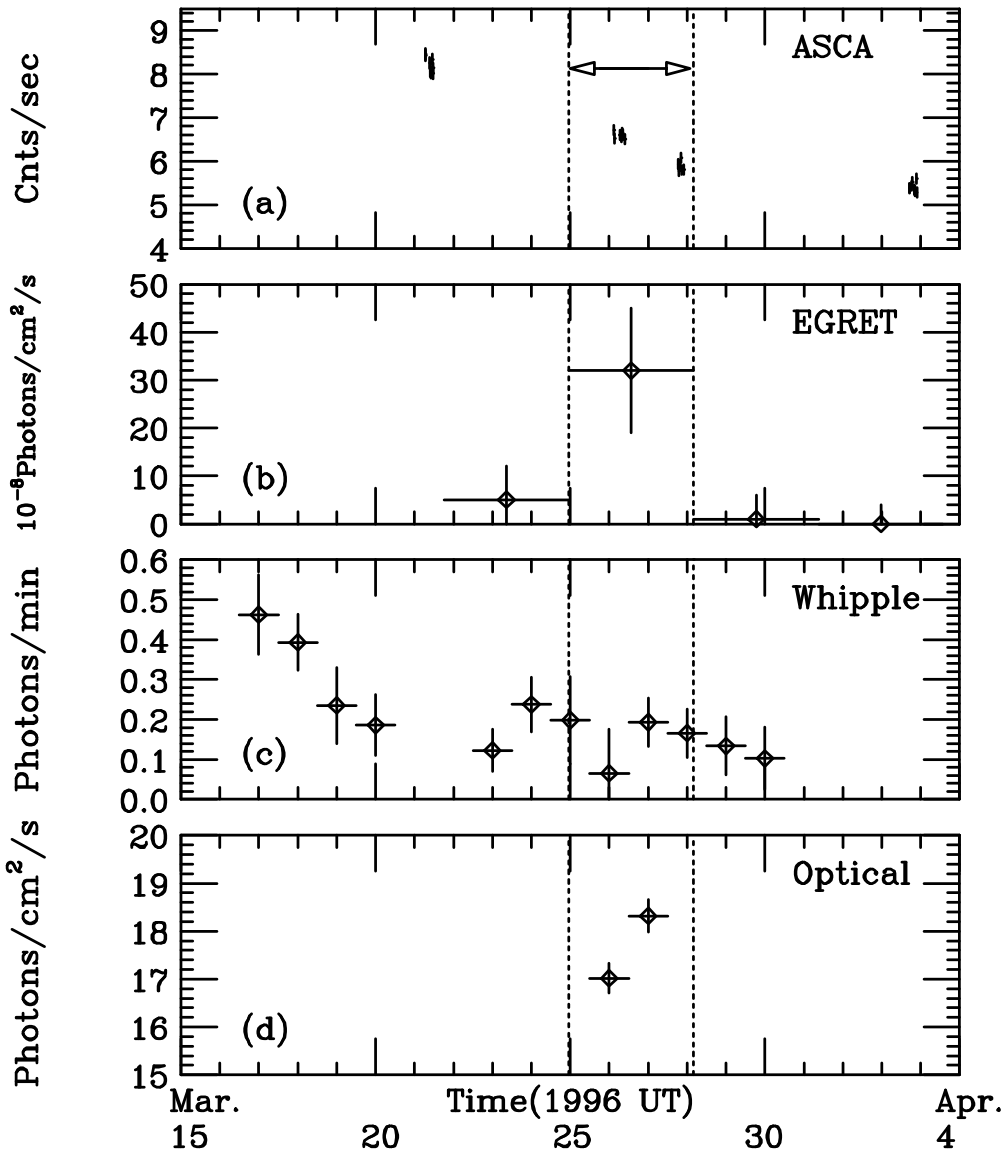

Fig. 1.— Time history of Mrk 501 during the March 1996 campaign. (a): X–ray (*ASCA*: 0.7 – 10 keV), (b): GeV (*EGRET*: 100 MeV – 10 GeV), (c): TeV (*Whipple*: above 350 GeV) and (d): Optical (R – band: 650 nm). The *ASCA* count rates are from the summed SIS0 and SIS1 data, extracted from a circular region centered on the target with a radius of 3 arcmin. The time interval marked with arrows is when *EGRET* detected Mrk 501 at 3.5 σ significance for the first time. All errors are 1 σ.

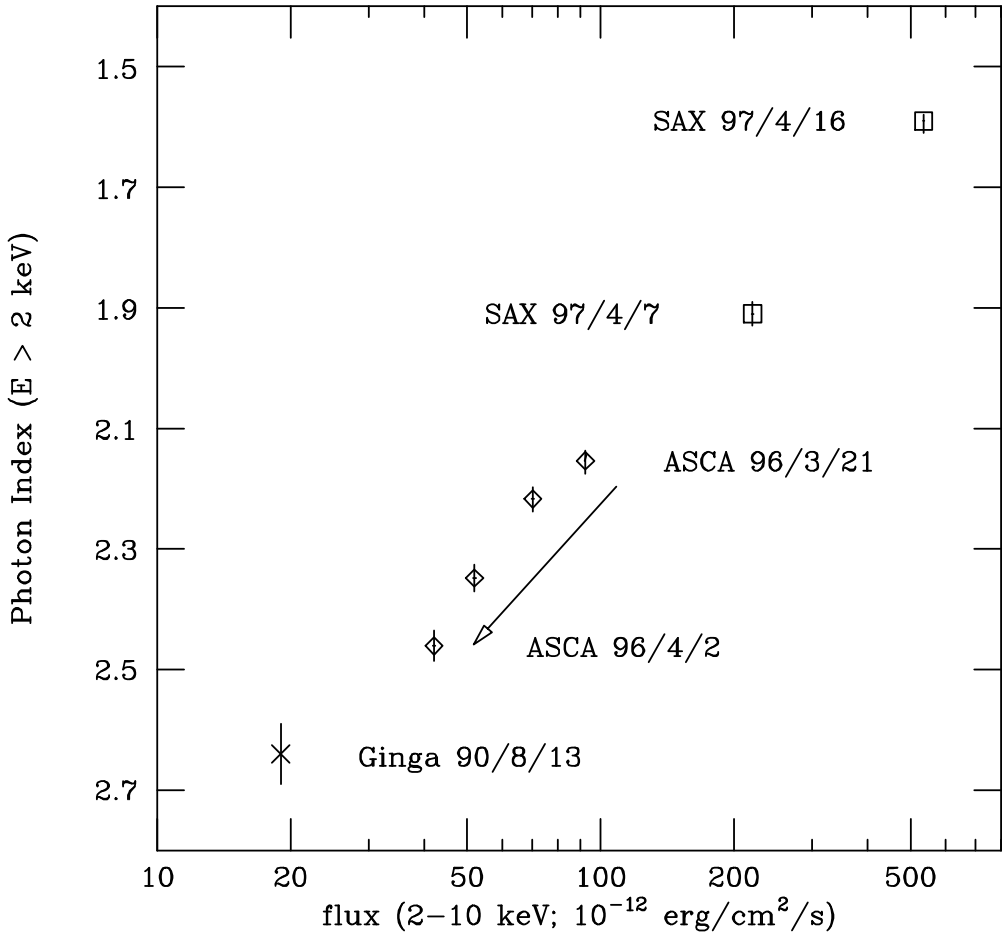

Fig. 2.— Correlation between 2–10 keV flux and spectral photon index above 2 keV for Mrk 501. *Ginga* and *BeppoSAX* results are respectively from Makino et al. (1991) and Pian et al. (1998). All errors are 1 σ. Arrow indicates an evolution during the *ASCA* observation in March & April 1996.

Fig. 3.— Maximum likelihood map of *EGRET* observations using photons above 500 MeV. The smaller PSF at higher energies yields good positional identification with Mrk 501 while clearly ruling out association with other nearby blazars.

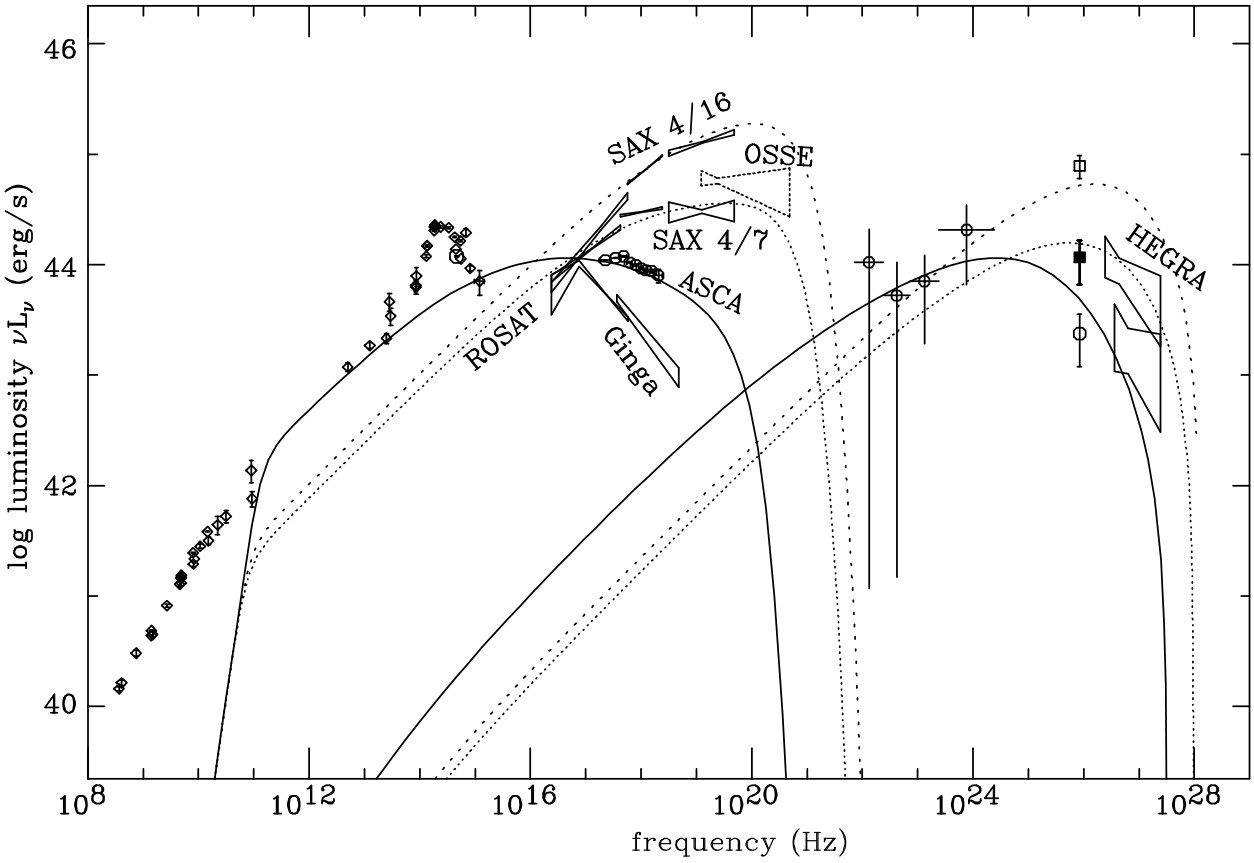

Fig. 4.— Multiband spectrum of Mrk 501. Circle: March 25 – 28 1996 campaign. Open Square: *Whipple* flux on April 16, 1997. Filled Square: *Whipple* flux on April 7, 1997. Diamond: non-simultaneous data from the NED data base. *ROSAT* (Comastri et al.1997), *Ginga* (Makino et al. 1991), *BeppoSAX* (Pian et al. 1998), *OSSE* (Catanese et al. 1997), *EGRET* (this work), *Whipple* (Quinn et al. 1996; Catanese et al. 1997) and *HEGRA* (Bradbury et al. 1997; Aharonian et al. 1997). *OSSE* data are average flux from April 9 to April 15, 1997. The lower *HEGRA* plots are averages from March to August 1996, while the upper plots are averages from March 15 to March 20, 1997. Both statistical and systematic errors are included in the *HEGRA* plots. The solid line corresponds to our model for the spectrum in March 1996, the dotted line for the data on April 7 and the line with small dashes for April 16 in 1997.

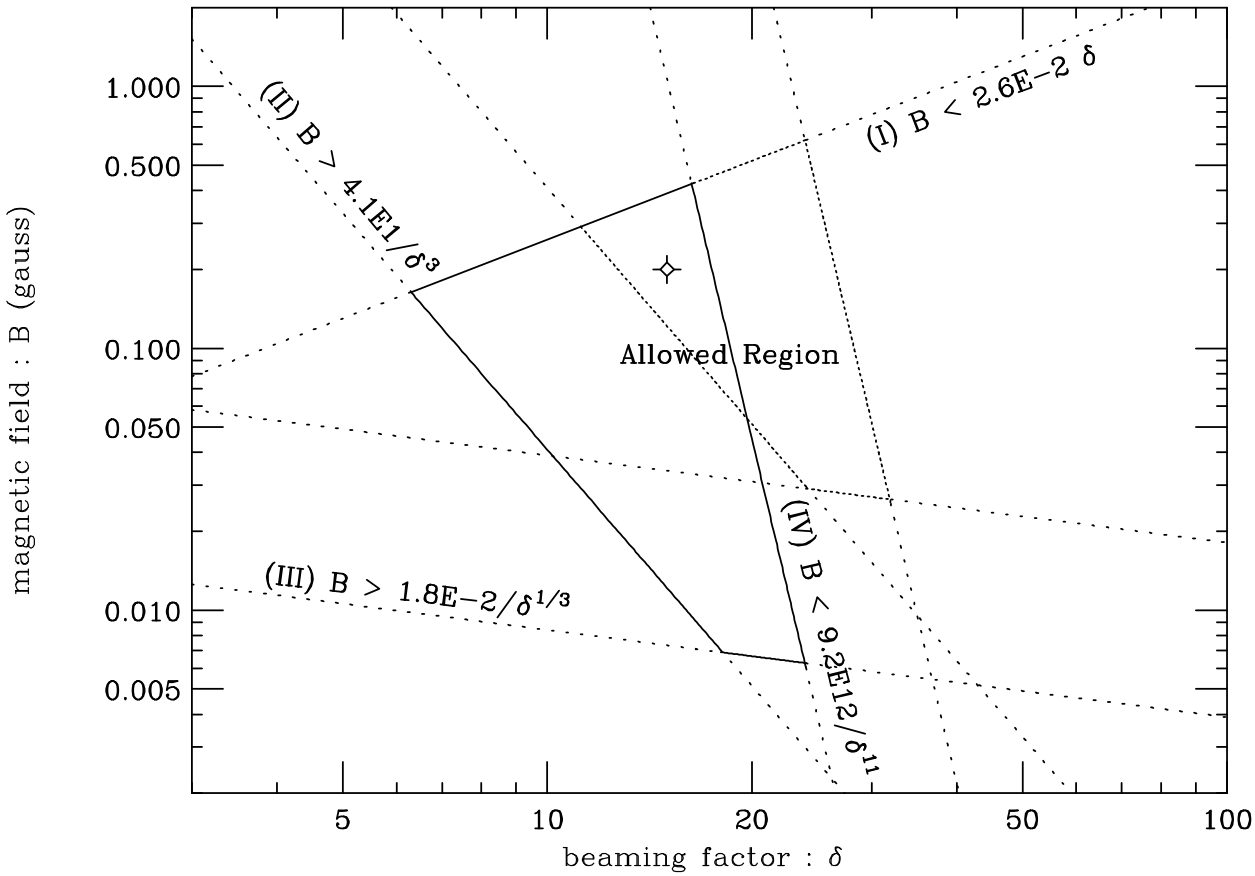

Fig. 5.— The parameter space (B, δ) allowed by the one-zone SSC model for Mrk 501 data. The figure surrounded with solid line is the allowed parameter space for variability time scale $t_{var} = 10^5$ sec and the cross point is the parameter used for our model (Figure 4). The figure with dotted lines is the allowed parameter space for $t_{var} = 10^4$ sec. Small dashes are constraints from each equations described in §4 for the case of $t_{var} = 10^5$ sec and $t_{var} = 10^4$ sec. (I) derived from the maximum energy of synchrotron emission (assumed here to be 50 keV) and Comptonized spectrum (E > 10 TeV). (II) derived from the observed luminosity ratio of the synchrotron and Inverse Compton components. We used here $l_{sync} \sim l_{SSC} \sim 10^{-10}$ erg cm^{-2} s^{-1}. (III) derived from the evaluation of the synchrotron cooling time (t_{sync}) and the variability time scale in the jet frame ($t_{var}\delta$). (IV) derived from the evaluation of the Compton cooling time (t_{SSC}) and the variability time scale in the jet frame. In the process of (I), we utilize non-contemporaneous data. Note that the equation of γ_{max} derived in (I) is subsequently used in (III) and (IV).